Analysis of porous NiTi shape memory alloy fabricated by MIM and SHS

X. W. GONG[*,a], L. X. ZHANG[b], Y. ZHANG[a], Q. SHI[a]
[a]*School of Naval Architecture and Ocean Engineering, Zhejiang Ocean University, Zhoushan, Zhejiang, 316022, P.R. China*
[b]*Research Institute of Baosteel, Baosteel Group, Shanghai, 200122, P.R. China*

In this paper, we study the porous NiTi shape memory alloy (SMA), fabricated by metal injection molding (MIM) and self-propagating high-temperature synthesis (SHS). To analyze the performance of the porous NiTi SMA, we used a scanning electron microscope(SEM), pore diameter distribution, composition, a differential scanning calorimeter(DSC), compression stress-strain curve, and more. The results showed that the porous NiTi alloy fabricated by MIM and SHS had greater porosity, generally more than 60%, with the pores divisible into two types, based on size: big pores, with a diammeter of approximately 1mm, and small pores, with a diameter of approximately 0.1-0.2mm. The NiTi main phases of B2 and B19´ and the tiny $NiTi_2$ middle transition phase were found in the porous NiTi shape memory alloy, but Ti and Ni pure element was not found in the product. While there was thermal imbalance in the self-propagating high-temperature synthesis process, it had little influence on the phase transformation point. The maximum compression resistance stress of the sample alloy reached 250MPa, and its extreme compression ratio reached 18%.

(Received August 3, 2014; accepted February 10, 2016)

Keywords: Metal Injection Molding(MIM), Self-propagating High-temperature Synthesis(SHS), Porous NiTi alloys, Shape memory, Performance analysis, Scanning Electron Microscope (SEM), Differential Scanning Calorimeter (DSC)

1. Introduction

Shape memory alloys (SMAs) represent a new functional material with driving functions, due to their shape memory effect (SME) and super elasticity (SE). With their unique SME and excellent mechanical properties, SMAs have been successfully employed in the manufacture of such products as thermo-sensitive elements, robot joints, micromechanics, mechanical springs, and valves [1-6]. Porous SMAs are lighter and have higher porosity than general SMAs, meaning they are conducive for the growth of newly born bone tissues and promote alloy biocompatibility. In 1994, Ukrainian researchers Gjunier et al. first fabricated the porous NiTi (nickel-titanium) SMA, which was used as bone replacement material. Current research reveals a promising application prospect for porous NiTi SMAs [7-9].

The fabrication of porous NiTi SMAs includes two main phases: molding and sintering. Some scholars have successfully synthesized porous NiTi SMAs by implementing self-progagating high-temperature synthesis (SHS) after powder compacting [10-12]. The traditional process of compacting metal powder is limited in the formation of product shapes, making mass production of titanium alloys with complex shapes by this means very difficult. This obstacle can be overcome, however, with metal injection molding (MIM) technology. Because MIM technology can economically and efficiently produce components with complex shape features on a large scale, it has unparalleled advantages compared over traditional powder metallurgy, casting and machining approaches [13-15]. The widely used methods for the sintering synthesis of porous NiTi SMAs are the normal sintering process, hot isostatic pressing (HIP), and self-propagating high-temperature synthesis (SHS), etc. SHS can best produce porous SMAs of high porosity, large pore size, and high purity, thus eliminating such problems as low porosity and uneven texture faced when other fabrication methods are employed. Many scholars adopt SHS to fabricate porous NiTi SMAs, which show anisotropic pore distribution, with porosity reaching 65% and higher [16-22].

At this point, little literature can be found on combining MIM and SHS to fabricate porous NiTi SMAs of high porosity. Therefore, we adopt an innovative method combining MIM and SHS to investigate the porous SMAs of high porosity and conduct detailed testing and analysis of the porosity, pore size, composition, and mechanical properties of the products. The purpose is to comprehensively master the synthesis of porous NiTi SMAs of high porosity by combining MIM and SHS, thus providing a helpful reference for their future mass production.

2. Experimental methods and process

In this research, the methods of MIM and SHS were adopted to synthesize porous NiTi SMA of high porosity. According to reference [23], the MIM process is shown in Fig. 1. A paraffin-based binder of low oxygen content was adopted, the mass ratio of the feed Ni:Ti:binder=55:45:25. First, nickel and titanium powders were put into the self-made powder mixer and mixed evenly for three hours. Second, the mixture of nickel and titanium powders and binder was tempered at 383-393K for two hours, after which it was loaded into the injection molding machine to obtain the blank sample. The debinding process included two steps: solvent debinding and thermal debinding. The injection blank after debinding was sintered with SHS method at preheating temperature of 300-500℃ and temperature rise speed of 10-15℃/min.

According to references [24,25], the SHS furnace is shown in Fig. 2. The electric heating wire and transformer heated the furnace, and the temperature was controlled by adjusting the output power of relay and transformer. The combustible component was placed in the furnace and ignited by a tungsten spark coil, with the preheating temperature of the blank sample controlled at 573K or 773K for one hundred to two hundred minutes. We adopted tungsten coil with a diameter of 1.0mm, along with low voltage and high current (supply voltage not above 25V and maximum current not above 70A). The spark coil in the incandescent state was controlled at 2273K or higher. Argon shielding tungsten wire was ignited directly on the powder sample (20×20×100 mm) surface. In order to eliminate the radiation effect of spark coil's ignition section on the blank sample side-surface, that surface's ignition section was enclosed with refractory bricks.

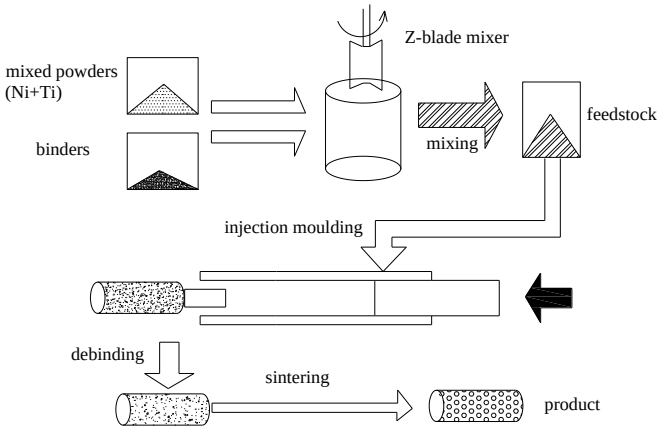

Fig. 1. Process of the metal injection molding [23]

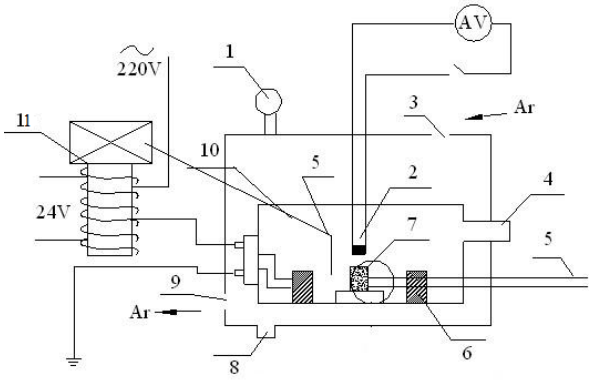

Fig. 2. Schematic diagram of the experimental apparatus for SHS porous NiTi SMA [24,25] 1. Pressure gage; 2. Tungsten wire coil; 3. Air inlet; 4. Observation well; 5. Thermocouple; 6. Preheating furnace; 7. Perforated pipe pattern; 8. Vacuum orifice; 9. Exhaust vent; 10. Reaction chamber; 11. Temperature relay

3. Results and discussion

3.1 SEM of porous NiTi SMA

Fig. 3 shows SEM pictures of a sample of the porous NiTi SMA with high porosity, fabricated at preheating temperature of 573K and 773K, respectively. According to the figure, the sintering reaction is thorough, with pores irregularly shaped mostly throughout and pore size increasing correspondent to preheating temperature. The higher the preheating temperature and the greater the melted fraction in the combustion process, the larger the pores become. In the testing for this study, porosity reached 60-70%, with pores divisible, by size, into two types: big pores, with a diameter of approximately 1mm, and small pores, with a diameter of approximately 0.1-0.2mm. Li Bingyun [12] et al. synthesized porous NiTi SMA by means of powder compacting and SHS, obtaining a porosity of approximately 40% and pore diameter of approximately 0.1-0.2mm at 823K preheating temperature. Therefore, it can be obtained that porous NiTi SMA sintered by MIM and SHS had higher porosity and greater pore size than that based on powder compacting molding and SHS. This can be explained by the large number of pores formed in the debinding process for MIM, leading to higher porosity and greater pore size in SHS process.

Since the porous NiTi SMAs fabricated according to the above-mentioned method have large pore size and high porosity, they are lighter in weight and higher in specific strength, displaying superiority in the fields of biomedical implant and bone replacement materials. Porous SMAs of high porosity and large pore size are more conducive for transmitting the nutritional ingredients of the human body fluid, thus potentially promoting the growth of mineralized and fibrous tissues into the bones, enhancing their connection with the peripheral tissues.

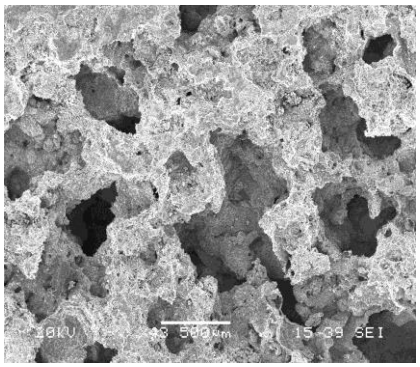

(a) Preheating temperature 573K

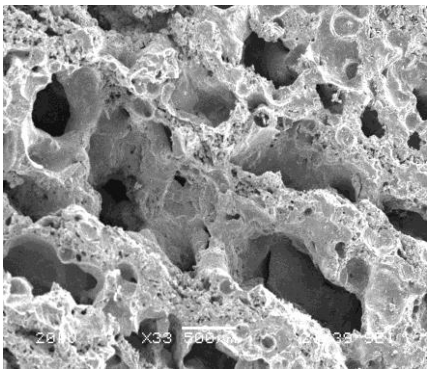

(b) Preheating temperature 773K

Fig. 3. SEM macrograph of the porous NiTi SMA

3.2 Pore diameter distribution of porous NiTi SMA

Fig. 4 shows the pore diameter distribution of porous NiTi SMA, obtained with a model 9500 mercury injection apparatus, produced by Micyomeyific. The Preheating temperature are, for Fig. 4(a), 573K and, for Fig. 4(b), 773K. These figures show that pores can be divided into two types, based on size: big pores, with a diameter of approximately 1mm and small pores, with a diameter of approximately 0.1-0.2mm. Big pores are mainly formed in the sintering process due to substantial pore formation inside the injection blank sample in the debinding process. Small pores, on the other hand, are primarily formed due to mutual diffusion of powder particles in the sintering process, which is similar to the compacting molding sintering process. The conclusion can be drawn, based on Figs. 4(a) and (b), that as the preheating temperature rises, the diameter of big pores gradually increases while that of small pores gradually decreases. This happens because higher preheating temperature enlarge the melted fraction in the combustion process, the melted fraction then encircles the alloy frame, and resulting in the formation of a large number of gradually enlarging pores in the injection blank sample in the debinding process. It also inhibits the formation of pores with a diameter of 0.1-0.2mm.

Employing this metal forming process and enhancing the preheating temperature can promote the fusion of small alloy pores into large ones, thus enhancing the pore size and porosity of the porous alloy products. This can play a positive role in endorsing the application of the porous SMAs.

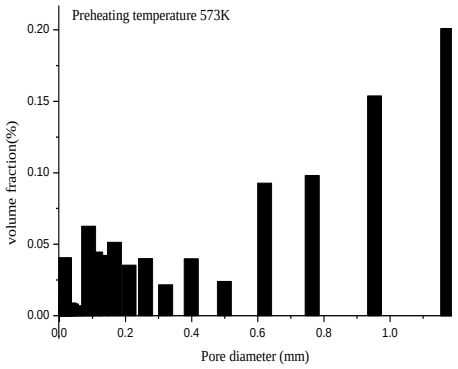

(a) Preheating temperature 573K

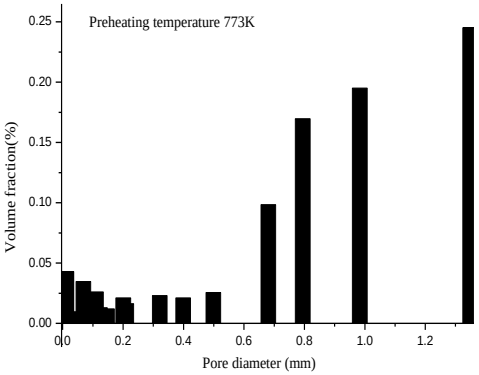

(b) Preheating temperature 773K

Fig. 4. Column map of pore size distribution of the porous NiTi

3.3 Composition analysis of porous NiTi SMA

Fig. 5 shows X-ray diffraction (XRD) curves of the porous NiTi SMA sample obtained with D/max-2200/PC test equipment, which is produced by Rigaku, Japan. The preheating temperature was controlled at 573K in Fig. 5(a) and 773K in Fig. 5(b). As shown in this figure, the NiTi main phase of B2 and B19´ and the tiny NiTi2 middle transition phase were found, but Ti and Ni pure element was not found in the product, indicating a perfect sintering reaction. These cases illustrate that although the reaction of Ti and Ni powders lasts for only a few seconds of the SHS process, compared to the powder diffusion sintering process, which can last dozens of hours, the combination reaction between element powders is perfect.

This method fully retains and demonstrates the advantages of SHS, such as high efficiency and savings of time and energy. Powder metallurgy and the infiltration

casting process both incur several challenges, such as a long production cycle, high energy consumption, and a complex process, these combined methods leading to high fabrication cost. SHS, however, compensates for these deficiencies. An analysis of Figs. 5 (a) and 5 (b) reveals that when preheating temperature is enhanced, the content of the B_2 phase increases gradually. That is because the higher the preheating temperature, the higher the sintering temperature, which leads to the higher B_2 diffraction peak.

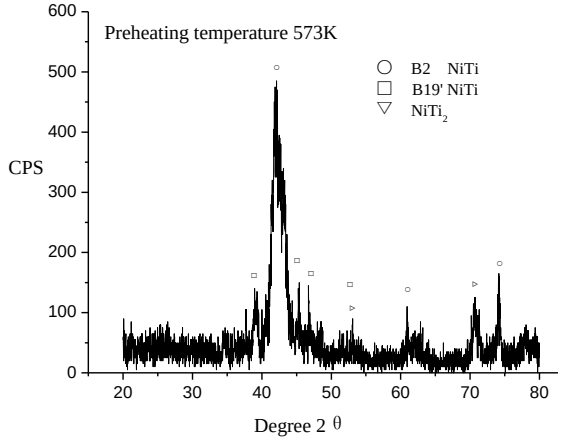

(a) Preheating temperature 573K

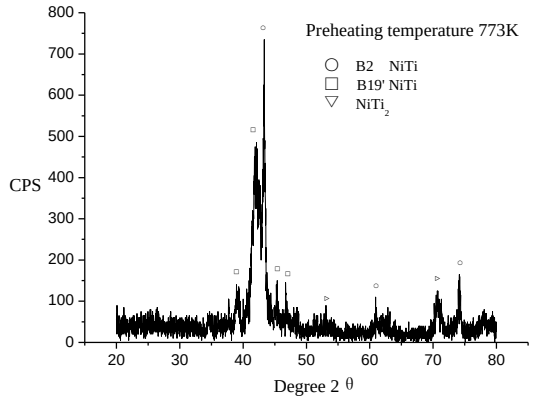

(b) Preheating temperature 773K

Fig. 5. XRD pattern of the porous NiTi SMA

3.4 DSC analysis of porous NiTi alloy

Fig. 6 contains differential scanning calorimeter (DSC) curve of the porous NiTi SMA obtained with Pyris1 equipment, produced by Perkin Elmer. Fig. 6(a) shows the process of martensite inverse phase transformation and Fig. 6(b) shows the process of martensite phase transformation, both at a preheating temperature of 573K. These two curves indicate combustion in the former part and latter parts of the SHS process, showing, moreover, that thermal imbalance in the SHS process has little influence to the phase transformation point. As shown in Fig. 6(a), martensite inverse phase transformation at the former and latter parts of the combustion is completed at A_f=343K and A_f=340K, respectively. In Fig. 6(b), the two peaks that appear in the cooling process indicate the existence of two phase transformations: parent phase → R phase and R phase → martensite phase transformation. In addition, martensite phase transformation at the former and latter parts of the combustion is completed at 297K and 299K, respectively, indicating even composition. DSC testing results are consistent with XRD testing results, and the samples keep in the coexistence region of parent phase and martensitic phase in normal temperature conditions.

The SME of the porous NiTi SMAs is related to the solid-state transformation between the martensite and the austenite, which could result from the heating up and cooling processes. With their excellent biocompatibility, unique SME, and super elasticity, porous NiTi SMAs offer a wide array of medical applications.

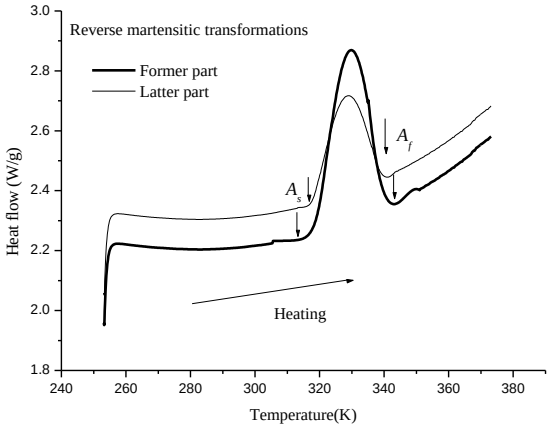

(a) Reverse martensitic transformations

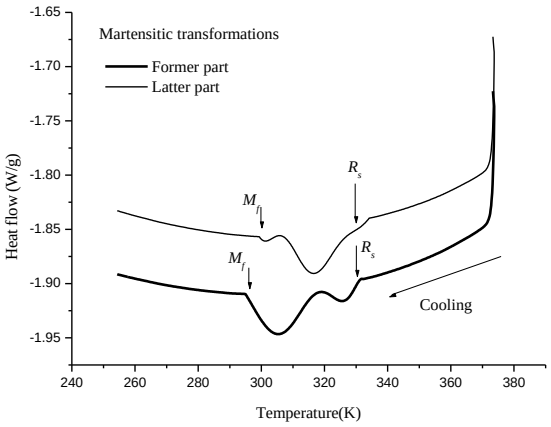

(b) Martensitic transformations

Fig. 6. DSC charts of the porous NiTi SMA

3.5 Compression performance analysis of porous NiTi alloy

Fig. 7 shows the compression performance of porous NiTi SMA, with porosity of approximately 67% at

preheating temperature of 773K. It has been well-established previously that the stress distribution of porous materials rises as strain, along with the compact materials, increases in the cold deformation process. According to Fig. 7, the stress-strain curve is divided into three stages: First is the obvious linear elastic stage, in which the sample is bent or compressed elastically. Second is strain yield, a stage during which the stress reaches a maximum of 250MPa through plastic deformation or buckling. Finally, the sample is damaged at the last stage, its limited compression ratio reaching up to 18%. Pores are also involved in the entire process of compression deformation.

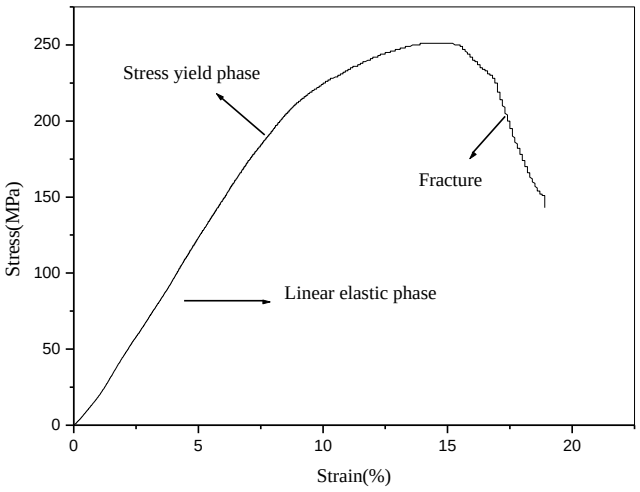

Fig. 7. Compression Stress - Strain Curve of Porous NiTi SMA

Fig. 7 does not show a similar compression platform for compressing compact NiTi alloy. As for compact NiTi alloy, under pressure, the force on the entire alloy is relatively even. When the external force exceeds the elastic range of the alloy strain, the alloy will entirely deform through the martensite, induced by the martensite's reorientation or the stress. Thus, when strain is enhanced, the stress of the alloy remains constant, forming a platform on the curve. As for the porous NiTi SMAs, however, the entire alloy deformation is achieved primarily through the big deformation induced by stress concentrated at the edge of pore wall. Under the same applied loading, stress is concentrated at the edge of the pore wall of the porous alloy, leading to plastic deformation. Due to coordinating effects between the pores, the strain at the center of the pore wall is relatively small. Even when the pore collapses or even breakage occurs within porous NiTi SMAs, the majority of the area at the center of pore wall is still substantially behind the plastic deformation stage. The force remains within the elastic range, applied stress not reaching the critical slippage stress of the martensite. Thus, the martensite does not reorient, and there is no yielding platform on the compression curve of the porous NiTi alloys. Therefore, if the shape of the pores can be adjusted to control the process parameters during the fabrication of porous NiTi SMAs, thus reducing stress concentration, the yield strength of the alloys can be enhanced, the maximum compression strain can be increased, and the mechanical properties of porous NiTi alloys can be improved.

4. Conclusions

This paper describes how we have adopted the methods of MIM and SHS to fabricate porous NiTi SMAs, and conducted detailed testing and analysis of the porous NiTi SMAs, including SEM, pore size distribution, XRD alloy composition, DSC, and alloy compression performance. The properties of the porous NiTi SMAs fabricated by this method have been analyzed. The following conclusions have been reached: (1) Combining MIM and SHS provides a helpful approach for fabricating porous NiTi SMAs. The MIM method can be used to produce many biomedical products with complex structures, and the SHS method offers such advantages as energy savings, time savings, and high efficiency. Combining the two can produce porous alloys of high porosity and large pore size, which can promote wider application of the porous NiTi SMAs in the biomedical fields. In this paper, the alloys fabricated by this method reached a porosity of 60~70% and maximum pore size 1mm, both larger than those of the NiTi SMAs fabricated by the traditional powder compacting and SHS. (2) The NiTi main phases of B2 and B19′ and the tiny $NiTi_2$ middle transition phase were found in the products of the SHS. The inverse martensitic transformation finishing temperature was approximately 340K. The two phase transformations occur in the cooling process: parent phase → R phase and R phase → martensite phase transformation. At room temperature, the sample is in the coexistence region of parent phase and martensite phase. (3) The entire deformation of the porous NiTi SMA was achieved primarily through by the large deformation induced by stress concentration at the edge of pore wall. No yielding platform was found on the compression stress-strain curve of the porous NiTi SMAs. When the fabrication process parameters are controlled, the shape of pores could be adjusted to reduce stress concentration, accordingly enhancing alloy yield strength, increasing the maximum compression strain, and improving the mechanical properties of the porous NiTi SMAs.

Acknowledgements

The authors gratefully thank financial supported by the National Natural Science Foundation of China (No. 51179174), Natural Science Foundation of Zhejiang Province (No.Y5100180), Academic Climbing Project of Zhejiang Educational Committee (No.pd2013221).

References

[1] Kazauhiro, Otsukr, X. B. Ren, Intermetallic, **7**, 511

(1995).
[2] R. Dominiek, V. B. Hendrik, Mechatronics, **8**, 635 (1998).
[3] J. G. John, H. Ken P. C. Greg, J Microelectromech S., **11**, 68 (2002).
[4] Z. G. Wang, X. T. Zu, X. D. Feng, J. Y. Dai, Mater. Lett. **54**, 55 (2002).
[5] J. H. Wang, F. Xu, S. Z. Yan, S. Z. Wen, J Tsinghua Univ (Sci & Tech), **43**, 188 (2003).
[6] L. Q. Wang, S. Y. Chen, W. P. Dai, L. W. Sun, L. L. Cheng, Fluid Machinery, **30**, 15 (2002).
[7] B. Y. Li, L. J. Rong, Y. Y. Li, Intermetallics, **8**, 643 (2000).
[8] B. Y. Li, L. J. Rong, Y. Y. Li, Metallurgy and Materials Transaction A, **31**, 1867 (2000).
[9] B. Y. Li, L. J. Rong, Y. Y. Li, Acta Materialia, **48**, 3895 (2000).
[10] X. M. Zhang, W. H. Yin, X. C. Wang, Rare Meta Mater. & Eng., **29**, 61 (2006).
[11] Y. H. Li, L. J. Rong Y. Y. Li, Chinese J Dialysis and Artificial Organs, **14**, 1 (2003).
[12] B. Y. Li, L. J. Rong, Y. Y. Li, V. E. Gjunter, Intermetallics, **8**, 881 (2000).
[13] R. M. German, Int. J. Powder Metall., **38**, 48 (2001).
[14] T. Barriere, B. Liu, J. C. Gelin, J. Mater. Process. Technol., **143-144**, 636 (2003).
[15] R. P. Koseski, P. Suri, N. B. Earhardt, R. M. German, Y. S. Kwon, Mater. Sci. Eng. A, **390**, 171 (2005).
[16] Z. A. Munir, U. Anselmi-Tamburini, Materials Science Report, **3**, 277 (1989).
[17] F. L. Zhang, Z. F. Yang, Y. M. Zhou, Int. Journal of Refractory Metals and Hard Materials, **29**, 344 (2011).
[18] Y. M. Zhou, F. L. Zhang, C. Y. Wang, Int. Journal of Refractory Metals & Hard Materials, **28**, 416 (2010).
[19] S. Gennari, U. A. Tamburini, F. Maglia, G. Spinolo, Z. A. Munir, Acta Materialia, **54**, 2343 (2006).
[20] A. M. Locci, A. Cincotti, F. Delogu, R. Orrù, G. Caoa, Chemical Engineering Science, **59**, 5121 (2004).
[21] M. J. Mas-Guindal, L. Contreras, X. Turrillas, G. B. M. Vaughan, A. Kvick, M. A. Rodríguez, Journal of Alloys and Compounds, **419**, 227 (2006).
[22] S. Gennari, F. Maglia, U. Anselmi-Tamburini, G. Spinolo, Intermetallics, **11**, 1355 (2003).
[23] R. M. German, A. Bose, Ed. by MPIF metal powder indutries federation, Princeton, New Jersey, USA. 1997, 1-100.
[24] S. Gennari, F. Maglia, U. Anselmi-Tamburini, G. Spinolo, Journal of Alloys and Compounds, **413**, 232 (2006).
[25] B. M. Khusid, V. V. Kulebyakin, E. A. Bashtovaya, B. B. Khina, International Journal of Heat and Mass Transfer, **42**, 4235 (1999).

*Corresponding author: gongwinfish@126.com